Original Russian Text © V. A. Pavlushin, A. A. Kubryakov, 2022,
published in MORSKOY GIDROFIZICHESKIY ZHURNAL, Vol. 38, Iss. 1 (2022)

Seasonal and Interannual Variability of the Thermohaline Structure of the Bengel Upwelling Based on the Argo Buoys Data

V. A. Pavlushin ✉, A. A. Kubryakov

Marine Hydrophysical Institute of RAS, Sevastopol, Russian Federation
✉ *pavlushin.92@mail.ru*

Purpose. The work is purposed at studying the water vertical structure in the Bengel upwelling region based on the Argo buoys data, its seasonal and interannual variability, as well as the possibility of using altimetry measurements to assess intensity of the eastern upwellings.
Methods and Results. Based on the Argo buoys measurements for 2004–2019, the spatial, seasonal and interannual variability of the Bengel upwelling thermohaline structure was investigated. With increase of depth, the zone of the deep water rise was observed to shear to the south and to the west. The maximum upwelling on the surface was recorded at latitude 25°S. However, the water rise in this zone was observed only up to the 300 m depth. At the same time, at latitude 30°S, the water rise was less intense on the surface, but was noted within the depth range 0–1500 m. Within the 100–600 m layer, seasonal variations of the temperature and salinity anomalies in the central part of the Bengel upwelling were almost the same.
Conclusions. Upwelling is most intense in July and weakens in April. At this time, the temperature and salinity anomalies within the 100–600 m layer reach 0.5°C and 0.05 psu, respectively. The secondary maximum of upwelling is observed in January in the 0–400 m layer, and its secondary minimum – in December. On the interannual scales (2004–2019), two periods of the upwelling significant weakening were recorded: in 2004–2005 and in 2018–2019.

Keywords: Bengal upwelling, seasonal variability, Argo buoys, interannual variability

Acknowledgements: the upwelling thermohaline structure was studied at the support of state task No. 0555-2021-0006 “Development of innovative methods, software, and the data processing and technical means of research of hydrophysical, biogeochemical, optical characteristics of marine environment including remote sensing methods”.

For citation: Pavlushin, V.A. and Kubryakov, A.A., 2022. Seasonal and Interannual Variability of the Thermohaline Structure of the Bengel Upwelling Based on the Argo Buoys Data. *Physical Oceanography*, [e-journal] 29(1), pp. 15-29. doi: 10.22449/1573-160X-2022-1-15-29.

DOI: 10.22449/1573-160X-2022-1-15-29

Introduction

Eastern boundary upwellings are part of the global oceanic conveyor, influencing the vertical exchange in the World Ocean. Water upwelling zones are the most important sources of nutrients contributing to the development of phyto- and zooplankton, which in turn are the food base for higher trophic levels. The research of the upwelling structure and variability is necessary to study the features of the thermohaline structure and bioproductivity of the ocean.

Along the southwestern coast of Africa between 34° and 15°S the Bengel upwelling (BU), one of the most productive regions of the South Atlantic, is located. BU structure was studied in a number of works based on episodic data from ship surveys [1–7]. These study results made it possible for the first time to characterize

the *TS* characteristics of water masses in the upwelling zone, the dynamics of currents and to study their spatial structure features [1–4, 8].

BU intensity and extent are characterized by pronounced seasonal and interannual variability. A large number of works are devoted to this study based on satellite data on the surface temperature [9–14]. However, satellite data provide information only about the characteristics of the surface, and do not permit to study the upwelling effect on deeper layers.

At the same time, there is very few data on the temporal variability of the vertical structure of the Bengel upwelling, especially in its deep-water part. In [5, 15], based on the data of a moored system installed at the130 m depth, the seasonal variation of salinity, temperature and current velocity in the coastal BU part is studiedIn particular, it was shown that the temperature and salinity in the entire studied water column (0–130 m) have a pronounced seasonal variation. The authors note the presence of two seasonal maxima and minima and attribute them to the influence of similar variability of alongshore currents. They contribute to the inflow/outflow of waters that have risen to the surface from the southern BU part [15, 16]. When analyzing the interannual variability of measurement data on moored buoys in 2002–2015, in [15] the appearance of positive temperature anomalies in 2007 and 2011 and negative ones – in 2004 and 2012 is noted.

However, an increasing temperature and salinity data amount in the study area becomes available owing to the Argo project. In the present paper, these measurements over more than 15 years are used for the first time to study the seasonal and interannual variability of the Bengel upwelling and its effect on the thermohaline structure of waters in the 0–2000 m water layer. It has been found that altimetry measurements make available the efficient estimate interannual changes in the thermohaline structure of the Bengel upwelling.

Data and Methods

The paper uses measurement data from Argo buoys in the area 5°–20°S and 15°–40°E for 2004–2018 obtained from the IFREMER archive (ftp://ftp.ifremer.fr/). The instrumental error of buoys is 0.002°C and 0.01 psu. Vertical resolution of these measurements in the upper layer varies from 10 to 1 m for different buoys. All data was visually checked for outliers, as a result of which a number of profiles with anomalously low salinity values and high temperatures in the lower layers were excluded from the array. In total, more than 17 thousand temperature and salinity profiles were obtained in the study area. To construct the spatial distribution, the data was linearly interpolated onto a regular grid with a 0.5° resolution.

The number of measurements has significantly increased since 2004 (500 profiles) – more than five times by 2018 (2500 profiles) (Fig. 1). Most of these measurements were carried out in the southern part of the study area. In the coastal part of the upwelling, there are relatively few measurements (10–20), since the buoys are quickly carried out of this part to the west under the influence of currents. Nevertheless, quite a lot of measurement data are available, obtained in the seaward part of the upwelling, where the number of profiles in a 1 × 1° cell is 60–90.

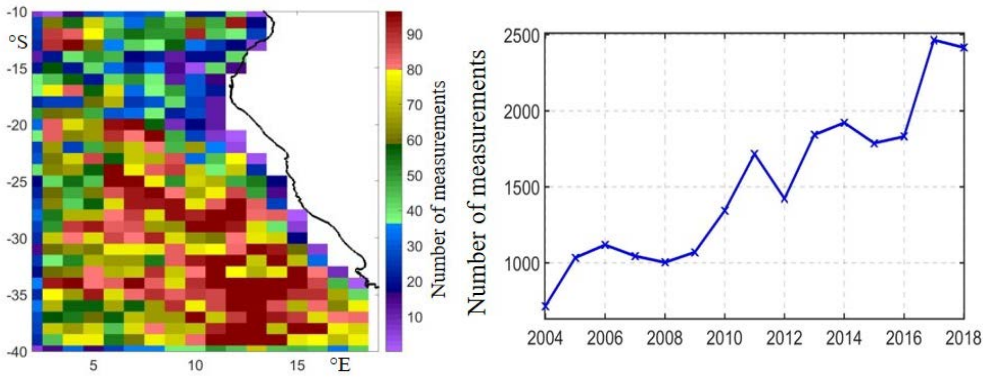

a *b*

F i g. 1. Spatial distribution of the Bio-Argo buoys measurements (*a*) and temporal variability in the number of measurements (*b*)

Spatial distribution of thermohaline characteristics in the upwelling area

Fig. 2 shows the average salinity and temperature field plotted according to Argo buoy data for 2004–2018 at 100, 300 and 600 m depths. Upwelling is distinguished as low temperature and salinity area near the western coast of Africa. At the 100 m depth, upwelling is pressed against the coast and represents a strip about 200–300 km wide with a salinity of about 35 psu and a temperature of 15 °C, which is 0.5 psu and 3 °C lower than in the central Atlantic (35.5 psu, 18 °C). At these depths, the coldest anomaly corresponding to the upwelling maximum is observed at 25°S latitudes in agreement with [13] based on satellite measurements of surface temperature.

With increasing depth, the upwelling region significantly increases both in width and meridional extent. So, at the 300 m depth, upwelling water with a salinity of 34.8 psu and a temperature of 10 °C at a latitude of 25°S stretch already for 400 km from the coast and are significantly extended to the northwest. Visually, the separation of waters of upwelling origin from the coast according to salinity data is observed at 20°S latitude (Fig. 2, *left*). The tongue of fresher upwelling waters in its northwestern part reaches the central South Atlantic at 20°S, 0°E. According to the temperature distribution (Fig. 2, *right*), this phenomenon is not so clearly observed, since the cold waters of the Bengel upwelling with a temperature of about 10°C join with the cold, but more saline waters of the equatorial upwelling. Difference in salinity and temperature between the upwelling region and the central part of the subtropical anticyclonic gyre at the 300 m depth is approximately the same as at 100 m, and is 0.3 psu and 3 °C, respectively. Note that the region of the lowest temperatures, i.e., the upwelling maximum, shifts with depth. At the 300 m horizon, the coldest anomaly is observed to the south than at the 100 m horizon, at a latitude of 28–30°S.

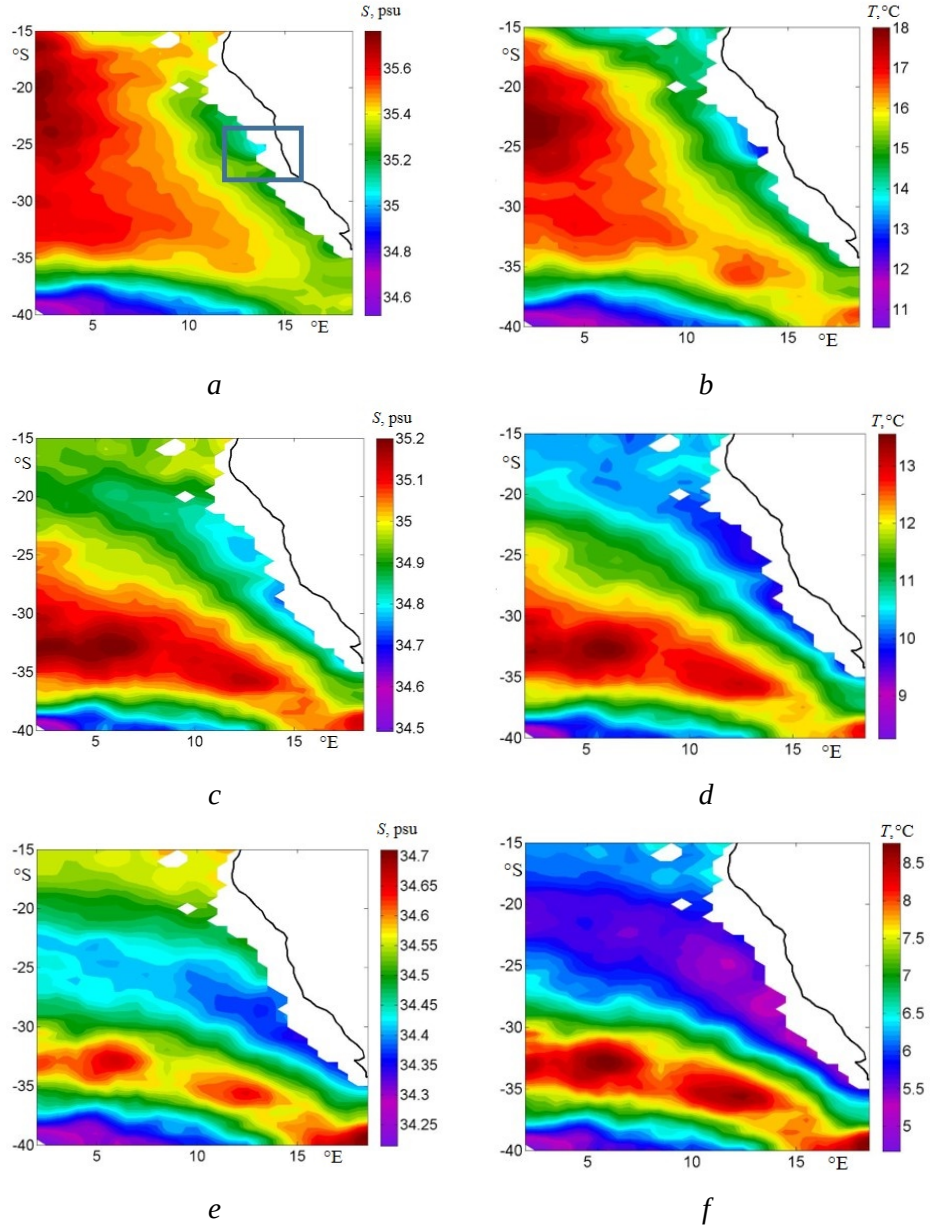

F i g. 2. Average distribution of salinity (*a*, *c*, *e*) and temperature (*b*, *d*, *f*) at the depths 100 m (*a*, *b*), 300 m (*c*, *d*) and 600 m (*e*, *f*) based on the Argo buoys data for 2004–2019

In deeper layers (deeper than 600 m), upwelling expands even more. In addition, the tongue of cold and fresher waters deviates more strongly from the coast to the west, in agreement with [17]. The waters at these depths are already several tenths of a degree colder than in the equatorial upwelling; they stand out both in temperature and in salinity. Thus, at the 600 m depth, the fresher water region width near the coast is about 500 km, and far from the coast it reaches 1000 km. Detachment of cold waters from the coast at these depths occurs to the south, at 25°S latitude.

Moving away from the coast, the area of fresher and colder waters expands, the temperature and salinity anomaly in it decreases. It indicates intensive processes of water mixing. On average, at these depths in the upwelling region, the salinity is 34.35 psu, and the temperature is 5 °C, which is 0.2 psu and 2 °C higher than in a narrow band south of the upwelling influence zone, which reflects the subtropical anticyclone region.

An idea of the vertical structure of upwelling is given by zonal sections of average temperature and salinity fields at depths up to 2000 m. For illustration, sections at 25°S and 30°S, corresponding to the maximum upwelling at depths of 100 and 300 m, respectively, are selected. For construction, data taken at a distance of ±0.5° from the central latitude of the studied section was used.

The rise of isohalines and isotherms near the coast is clearly seen in the middle sections in Fig. 3. The rise of waters in the upper 0–100 m layer is most clearly observed according to salinity measurements, since the seasonal variation of atmospheric heat fluxes has a great influence on the temperature distribution in these layers.

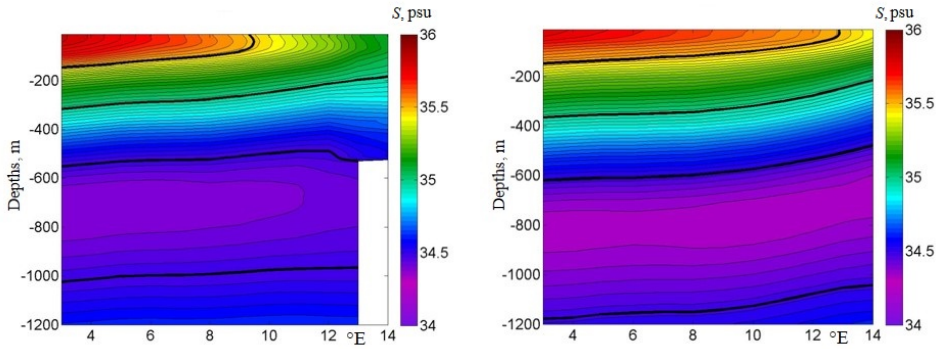

F i g. 3. Vertical sections of the salinity field at 25°S (left) and 30°S (right) in the 0–2000 m layer. The isohalines 34.5, 35 and 35.5psu are highlighted in black

The upwelling intensity in the surface layer reaches a maximum at 25°S. In this area, waters with a salinity of 35.2 psu come to the surface, pushing waters with a salinity of 35.8 psu into the central part of the ocean. On the section from 5°–14°E, 35.2 psu isohaline rises to the surface from a depth over 250 m. With depth at these latitudes, the intensity of the vertical uplift decreases. The 35 psu isohaline and the 8 °C isotherm rise from the 300 m depth to a horizon of 200 m. Below 300 m, the rise of isohalines and isotherms is replaced by their subsidence, i.e., downwelling at depths of 300–500 m in the coastal zone (12°–14°E) appears. Thus, in this area, water divergence is observed at depths of about 300 m, above which the closure of the vertical circulation cell occurs in the form of upwelling, and below it, in the form of downwelling.

At the 300 m depth, upwelling is most intense at 30°S. In this area, salinity and temperature near the coast are much higher than at 25°S latitude. Data from Argo buoys show that the rise of isohalines at 30°S latitude covers a much larger water

column. An important feature of the vertical distribution of salinity in the study area is the intermediate salinity minimum at depths of 600–800 m, below which salinity begins to increase [17]. Presence of an intermediate salinity minimum leads to the fact that above it, upwelling results in the rise of desalinated waters and the appearance of a fresh anomaly, and below it, – to an increase in salinity. Thus, the 35.2 psu isohaline rises 100 m from a depth of 600 m at a longitude of 9°E to the horizon 500 m near the shore. The same isohaline is located at a depth of 1100–1200 m and rises to 100 m near the shore. A similar rise is also observed according to temperature data (Fig. 4). Rise of saline waters is noted at 30°S latitude up to the maximum observation depth of 2000 m, where the 34.8–34.9 psu isohalines are located.

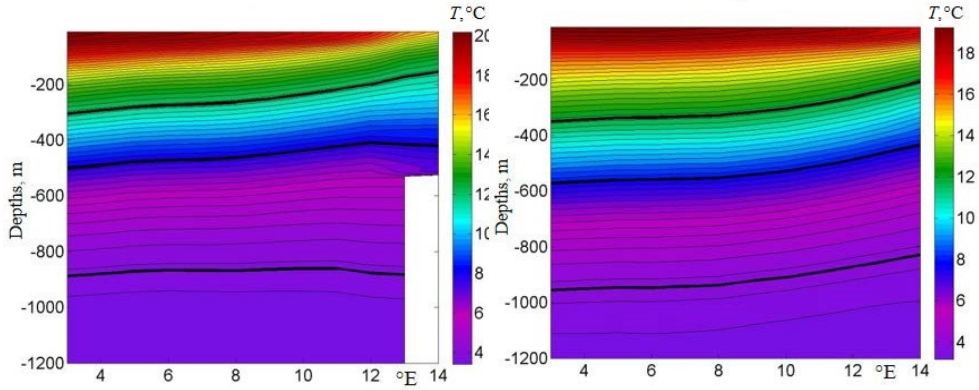

F i g. 4. Vertical sections of the temperature field at 25°S (*left*) and 30°S (*right*) in the 0–2000 m layer. The isotherms 7, 10, and 13 °C are marked out

Seasonal variability of the thermohaline structure of the Bengel upwelling waters

For the analysis of seasonal variability, an area with coordinates of 12°–16°E and 23°–28°S corresponding to the upwelling peak (see the selected rectangular area in Fig. 2) was chosen. The number of measurements in this area is 436 profiles. Fig. 5 and Fig. 6 show seasonal diagrams averaged over this area and profiles of salinity and temperature anomalies in certain months. The maximum negative temperature and salinity anomalies in the 200–600 m layer are observed in July–September, indicating upwelling intensification and the rise of deep desalinated and cold waters. Decrease in salinity in summer coincides with earlier data from [5]. At the same time, the spatial distribution of anomalies is approximately the same at depths of 250–550 m, and the maximum negative values are observed in July (about –0.5 °C and 0.05 psu) (Fig. 6). The second peak of the negative anomaly is observed in January-February. Unlike the autumn one, this peak falls on the upper 100–350 m layer. Such a semi-annual course of salinity anomalies was also noted based on contact measurements [5, 15].

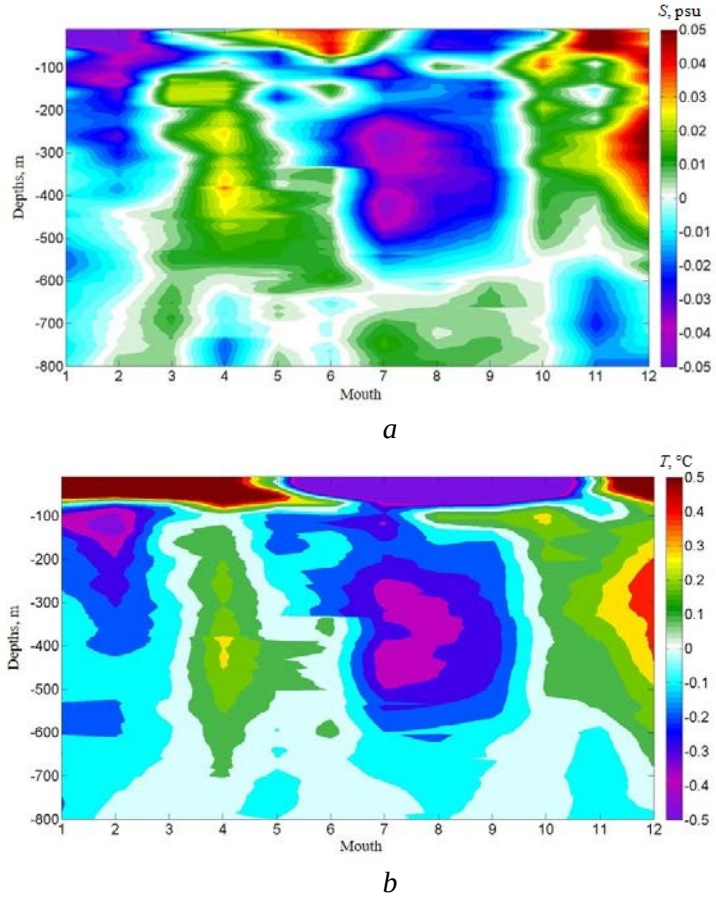

F i g. 5. Seasonal diagram of the salinity (*a*) and temperature (*b*) anomalies in the BA central part (see the marked out rectangular area in Fig. 2, *a*)

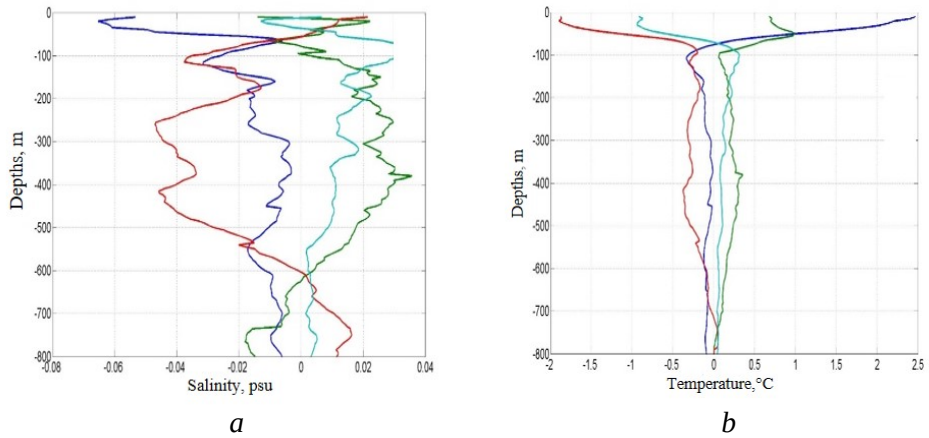

F i g. 6. Profiles of the salinity (*a*) and temperature (*b*) anomalies in January (blue line), April (green line), July (red line) and October (blue line) in the BA central part (12°–16°E and 23°–28°S)

The diagram shows that at depths over 600 m, the salinity anomalies change their sign. The change in sign is because salinity begins to increase below these depths (see Fig. 5, *a*). Increased upwelling leads to the rise of saline waters and an increase in salinity, rather than its decrease, as in the upper layers. Temperature anomalies in the lower layers are quite small, since the temperature gradients below 600 m are significantly weakened. The maximum positive anomalies corresponding to the upwelling weakening periods and lowering of isotherms are observed in April and December.

Note that in the upper 100-m layer, the interaction with the atmosphere has a decisive influence on the variability of thermohaline characteristics. Therefore, the seasonal temperature variation on the surface differs significantly from the variability at depths below 100 m. The maximum temperature and salinity anomalies are observed in the summer period from November to April, and the minimum ones, from May to October. Seasonal heating, in particular, masks the upwelling intensification in the surface temperature field in January-February, which is clearly observed according to Argo data at depths over 400 m.

Seasonal course of precipitation and evaporation can also have a significant effect on salinity in the upper 0–100 m layer. Seasonal curves of salinity in the upper and lower layers are qualitatively similar, since salinity is a more conservative parameter. Thus, it is salinity that is the most effective tracer of the upwelling intensity both in the upper and lower layers in accordance with [2].

For comparison, vertical sections of salinity in the month of maximum (July) and minimum (April) intensity of vertical water rise at 30°S latitude (Fig. 7) are considered. For clarity, the sections show 34.9, 35.1 and 35.3 psu isohalines. When comparing the right and left parts, Fig. 7 clearly shows that in July all the identified isohalines are higher than in April. The rise of isohalines is noted within 6°–15°E. Waters with a salinity of less than 34.9 psu during the period of intensified upwelling occupy a twice as large area about 200 km wide compared to April (100 km). Near the coast, the 35–35.1 psu isohalines rise by 30 m compared to April. In the deep layers, the seasonal rise is even more pronounced: for example, the 35.3 psu isohaline rises by more than 50 m.

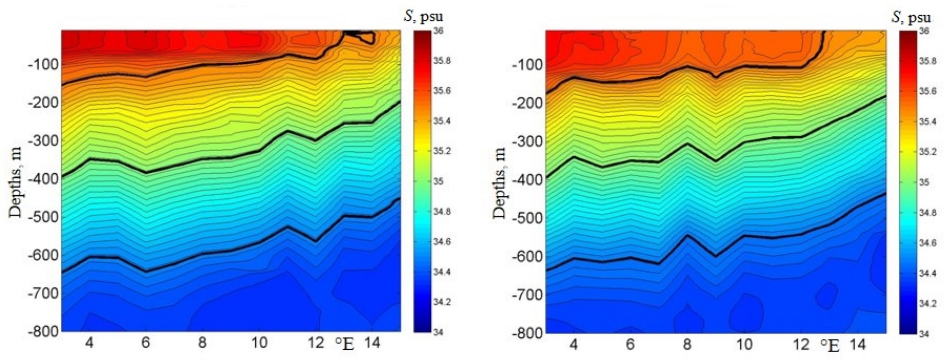

F i g. 7. Zonal sections of salinity at latitude 30°S for April (*a*) and July (*b*)

Fig. 8 and Fig. 9 show a diagram of salinity and temperature anomalies averaged for the central BU part (see the selected rectangular area in Fig. 2, *a*) and the variability of the average temperature and salinity anomaly in the 0–1000 m layer in 2004–2019. Anomalies were counted from the average value for the entire time period. Fig. 8 shows that the average salinity and temperature anomalies correlate well with each other. Vertical advection leads to a synchronous rise/fall of colder and fresher waters, so the variability of these parameters in the upwelling region is almost the same. Changes in average depth temperature by 0.1 °C in the upwelling area roughly correspond to a change in average salinity by 0.01 psu.

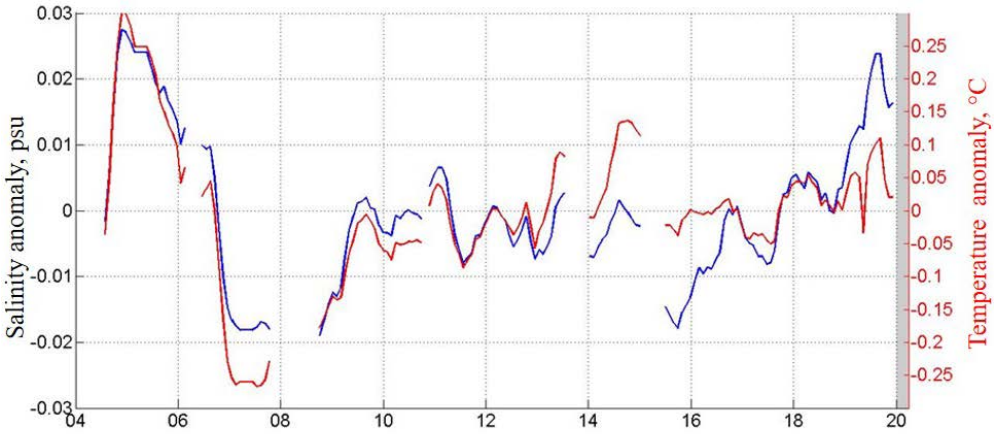

F i g. 8. Interannual (2004–2020) variability of the salinity and temperature mean anomalies in the 0–600 m layer in the BA central part (12°–16°E and 23°–28°S)

Note the significant interannual variability of thermohaline characteristics in the study zone. High anomalies were noted in 2004–2005, when there was an increase in temperature and salinity by 0.5 °C and 0.05 psu, respectively. These changes are recorded in the entire 0–600 m layer, indicating the upwelling weakening (Fig. 9).

In the next three years, namely, in 2007–2009, on the contrary, a sharp decrease in temperature and, as a result, in salinity was observed. The salinity and temperature anomalies in this layer were negative. At the same time, salinity below the 600 m level increased by 0.01 psu, reflecting the rise of deep saline waters. Thus, upwelling intensified during this period, and the intensity of the vertical rise was higher than the average for 2004–2019.

Two less intense upwelling weakening events were observed in 2010–2011 and 2014–2015. During this period, the temperature and salinity in the upper 600 m layer increased by 0.2 °C and 0.25 psu, respectively. As mentioned above, all active changes were observed almost uniformly in the 150–600 m layer.

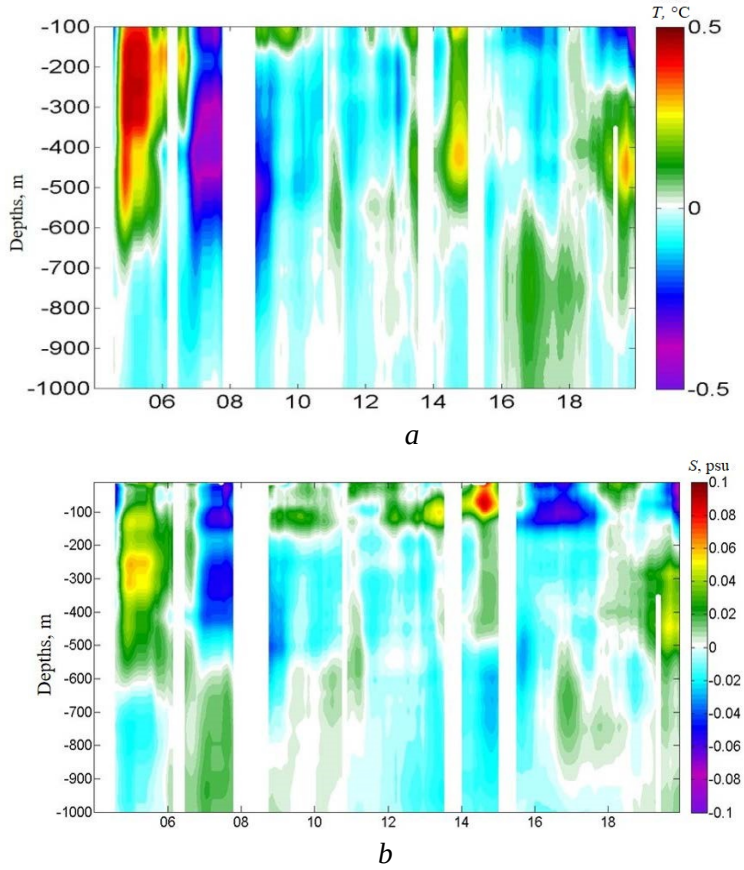

F i g. 9. Interannual variability of vertical distribution of the temperature (*a*) and salinity (*b*) anomalies in the BA central part (12°–16°E and 23°–28°S)

These results are consistent with such measurement data on moored buoys in the BU coastal zone [15], which show the appearance of positive temperature anomalies in 2004 and 2015 and negative anomalies in 2007 and 2012.

Another event with a sharp temperature and salinity increase at these depths was recorded in 2018–2019. At the same time, salinity anomalies are comparable with the data for 2005–2006. Thus, the Argo buoys data show that another phase of upwelling weakening is currently observed.

For an example Fig. 10, *a* and 10, *b* show the mean annual temperature anomalies for 2004 and 2011 calculated as deviations from the averaged satellite data for 1985–2016 from the temperature array [18] (Fig. 10, *a*, *b*) obtained from satellite infrared and microwave data.

It is clearly seen that due to the upwelling weakening in 2004 in the study area (highlighted by a rectangle in Fig. 10, *a* – *d*), the temperature anomaly was positive (0.2–0.4 °C). In 2011 (Fig. 10, *b*), on the contrary, increased upwelling led to a decrease in temperature and its anomalies reached –1 °C.

The Argo buoys measurements permitted to obtain estimates of the upwelling effect on the deep layers. Analysis of the temperature anomaly map according to the

Argo buoy data for the same years at a depth of 100 m (Fig. 10, *c*, *d*) shows similar results. Here, too, in 2004, the temperature rises by 0.8–1 °C, and in 2011, it falls by 1–1.2 °C.

The intensity of upwelling is primarily determined by the variability of wind intensity in the region.

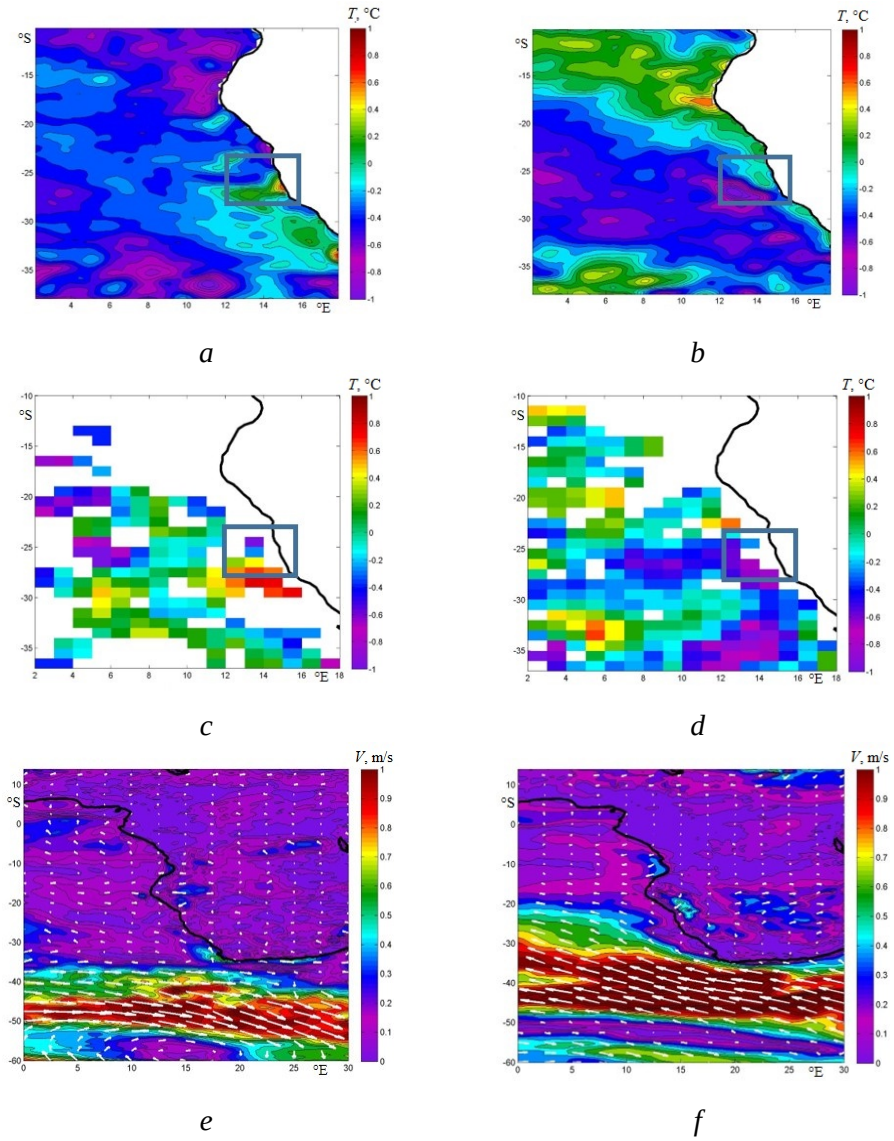

F i g. 10. Annual average anomalies of the satellite-derived temperature (*a*, *b*), the Argo buoys-derived temperature (*c*, *d*) and wind (*e*, *f*) in the Bengel upwelling region for 2004 (*a*, *c*, *e*) and 2011 (*b*, *d*, *f*)

On Fig. 10, *e*, *f* show maps of average annual wind anomalies for 2004 and 2011, calculated as deviations from the average climatic distribution for 1993–2018. In 2011 (Fig. 10, *f*), western winds intensify, contributing to the upwelling

development. On the contrary, the wind speed anomaly vectors in 2004 (Fig. 10, *e*) are directed in the opposite direction to the southeast. Such anomalies in wind speed indicate a weakening of the average winds this year, which leads to the upwelling intensity decrease.

Such changes are primarily caused by the displacement and weakening of a large-scale subtropical high in the atmosphere. A number of works have shown that such changes can be partially associated with El Niño events [12]. A detailed study of the causes of such atmospheric changes is beyond this work scope.

Non-uniformity of Argo buoy measurements in time and space can affect the obtained estimates of the variability of the thermohaline structure of waters. To compare the obtained estimates, the sea level data obtained from the measurements of satellite altimeters is used. The rise of deep cold waters causes an increase in density and, as a result, a drop in sea level. Upwelling intensification will cause a drop in sea level, and a weakening will cause it to rise. Thus, the change in the mean anomaly of temperature and salinity will be in phase with sea level. Changes in upwelling can also be associated with increased winds. In this case, as a result of the surge, the level will decrease, which will lead to upwelling and, as a result, a decrease in salinity.

Fig. 11 shows a comparison of the mean sea level and the mean salinity anomaly in the 600 m layer in the selected area. It is clearly seen that these series correlate well with each other. Increase in salinity because of weakening upwelling in 2004–2005, 2010–2011, 2014–2015 and 2018–2019 led to sea level rise, most intense in 2004–2005 and 2018–2019. A decrease in sea level and salinity due to increased upwelling occurs in 2008–2009 and 2012–2013.

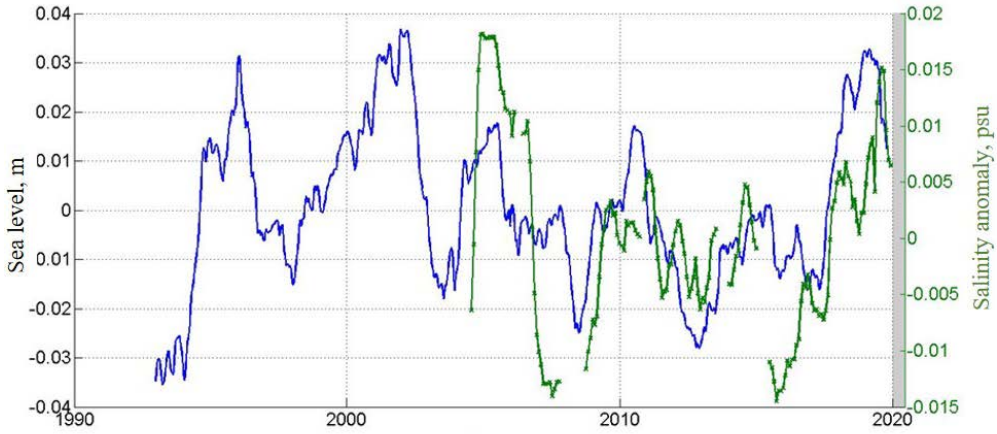

F i g. 11. Interannual variability of the altimetry sea level (blue line) and the salinity anomaly (green line) in the BA central part (12°–16°E and 23°–28°S)

The comparison in Fig. 11 shows that sea level is a good indicator of upwelling intensity and can be used to study the interannual upwelling variability. This data has been available since 1992 and allow the study of upwelling fluctuations over a long time period. According to Fig. 11, intense upwelling weakening events should

also have been observed in 1996–1997 and 2001–2002, and upwelling intensification, in 1998–1999, which coincides with the results of the SST analysis from a number of previous works [11, 12, 14]. Unlike the Argo buoy data, the altimetry measurements are regular; therefore, the coincidence of the series in the figure also indicates the reliability of the estimates obtained from the Argo buoy measurements.

Conclusions

In the present work, based on the use of a large array of hydrological measurement data (more than 30000), the seasonal and interannual variability of the thermohaline structure of the Bengel upwelling was analyzed. Based on the analysis carried out, it is shown that:

1) Maximum upwelling on the surface occurs at 25°S latitude. However, at this latitude, the water rise is observed only to depths of 300 m. At the same time, at 30°S latitude, water rise is recorded in the depth range of 0–1500 m, while on the surface it is less intense. In general, there is a tendency for the deep-water rise zone to shift south and west with increasing depth.

2) The seasonal course of the temperature and salinity anomalies is practically the same in the 100–600 m layer. Upwelling is most intense in July, when the temperature and salinity anomalies in the 100–600 m layer reach 0.5 °C and 0.05 psu. In April, a minimum of water rise is observed and the same magnitude anomalies of temperature and salinity are recorded. The secondary upwelling maximum is observed in January in the 0–400 m layer, and the secondary minimum is observed in December. It is noted that salinity is a more reliable tracer of upwelling intensity in the upper layer, since solar heating has a great influence on temperature.

3) For the first time Argo buoys measurement data made it possible to study the interannual variability of the upwelling thermohaline structure. On an interannual scale in 2004–2019, two periods of significant weakening of upwelling were recorded: in 2004–2005 and 2018–2019. In these years, an increase in the average annual temperature and salinity in the 100–600 m layer by 0.5 °C and 0.05 psu, respectively, is recorded, which is consistent with the measurement data on moored buoys. Increased upwelling, a decrease in temperature, and an increase in water density lead to the steric level drop.

4) This paper shows that altimetry level measurements in the upwelling area are in good agreement with the water salinity and temperature variability. Thus, regular altimetry measurements available since 1992 can be used to describe the interannual variability of the upwelling intensity. In particular, these measurements show that a significant weakening of upwelling was observed in 1996–1997 and 2001–2002, and its strengthening in 1998–1999.

REFERENCES

1. Shannon, L.V., Nelson, G. and Jury, M.R., 1981. Hydrological and Meteorological Aspects of Upwelling in the Southern Benguela Current. In: F. A. Richards, Ed., 1981. *Coastal Upwelling*. Washington, DC: American Geophysical Union, pp. 146-159. https://doi.org/10.1029/CO001p0146

2. Armstrong, D.A., Mitchell-Innes, B.A., Verheye-Dua, F., Waldron, H. and Hutchings, L., 1987. Physical and Biological Features across an Upwelling Front in the Southern Benguela. *South*

African Journal of Marine Science, 5(1), pp. 171-190. https://doi.org/10.2989/025776187784522559

3. Gordon, A.L., Bosley, K.T. and Aikman III, F., 1995. Tropical Atlantic Water within the Benguela Upwelling System at 27°S. *Deep Sea Research Part I: Oceanographic Research Papers*, 42(1), pp. 1-12. https://doi.org/10.1016/0967-0637(94)00032-N
4. Rae, C.M.D., 2005. A Demonstration of the Hydrographic Partition of the Benguela Upwelling Ecosystem at 26°40'S. *African Journal of Marine Science*, 27(3), pp. 617-628. https://doi.org/10.2989/18142320509504122
5. Mohrholz, V., Bartholomae, C.H., van der Plas, A.K. and Lass, H.U., 2008. The Seasonal Variability of the Northern Benguela Undercurrent and Its Relation to the Oxygen Budget on the Shelf. *Continental Shelf Research*, 28(3), pp. 424-441. https://doi.org/10.1016/j.csr.2007.10.001
6. Bukatov, A.E. and Solovei, N.M., 2017. Evaluation of the Density Field Vertical Structure and the Characteristics of Internal Waves Relation with Large-Scale Atmospheric Circulation in the Peruvian and Benguela Upwelling Areas. *Processes in GeoMedia*, (2), pp. 485-490 (in Russian).
7. Bulgakov, S.N., Bulgakov, N.P., Mikhailova, E.N. and Shapiro, N.B., 2005. Generation of Upwelling near the Pacific Coast of Mexico. *Physical Oceanography*, 15(1), pp. 27-36. https://doi.org/10.1007/s11110-005-0027-0
8. Malinin, V.N., Chernyshkov, P.P. and Gordeeva, S.M., 2002. *Canary Upwelling: Large-Scale Variability and Forecast of Water Temperature*. Saint Petersburg: Hydrometeoizdat, 156 p. (in Russian).
9. Timokhin, E.N., 2002. [Features of Intra-Annual and Interannual Variability of Fields of Hydrometeorological Elements in the Fishing Areas of the Southeast and Bengel Upwelling]. In: AtlantNIRO, 2002. *Proceedings of the XII International Conference on Fisheries Oceanology (XII ICFO)*. Kaliningrad: AtlantNIRO Publishing House, 2002. pp. 244-246 (in Russian).
10. Serebrennikov, A.N., 2019. [Method of Spatial Separation of Upwelling by the Nature of Seasonal Variability of Temperature and Wind Fields]. In: IPTS, 2019. *Environmental Control Systems – 2019: Abstracts of the International Scientific and Technical Conference, Sevastopol, September 12-13, 2019*. Sevastopol: IPTS, p. 129 (in Russian).
11. Hagen, E., Feistel, R., Agenbag, J.J. and Ohde, T., 2001. Seasonal and Interannual Changes in Intense Benguela Upwelling (1982–1999). *Oceanologica Acta*, 24(6), pp. 557-568. https://doi.org/10.1016/S0399-1784(01)01173-2
12. Hardman-Mountford, N.J., Richardson, A.J., Agenbag, J.J., Hagen, E., Nykjaer, L., Shillington, F.A. and Villacastin, C., 2003. Ocean Climate of the South East Atlantic Observed from Satellite Data and Wind Models. *Progress in Oceanography*, 59(2–3), pp. 181-221. https://doi.org/10.1016/j.pocean.2003.10.001
13. Chen, Z., Yan, X.-H., Jo, Y.-H., Jiang, L. and Jiang, Y., 2012. A Study of Benguela Upwelling System Using Different Upwelling Indices Derived from Remotely Sensed Data. *Continental Shelf Research*, 45, pp. 27-33. https://doi.org/10.1016/j.csr.2012.05.013
14. Lamont, T., García-Reyes, M., Bograd, S.J., van der Lingen, C.D. and Sydeman, W.J., 2018. Upwelling Indices for Comparative Ecosystem Studies: Variability in the Benguela Upwelling *System. Journal of Marine Systems*, 188, pp. 3-16. https://doi.org/10.1016/j.jmarsys.2017.05.007
15. Junker, T., Mohrholz, V., Siegfried, L. and van der Plas, A., 2017. Seasonal to Interannual Variability of Water Mass Characteristics and Currents on the Namibian Shelf. *Journal of Marine Systems*, 165, pp. 36-46. https://doi.org/10.1016/j.jmarsys.2016.09.003
16. Rouault, M., Florenchie, P., Fauchereau, N. and Reason, C.J.C., 2003. South East Tropical Atlantic Warm Events and Southern African Rainfall. *Geophysical Research Letters*, 30(5), 8009. https://doi.org/10.1029/2002GL014840

17. Stramma, L. and England, M., 1999. On the Water Masses and Mean Circulation of the South Atlantic Ocean. *Journal of Geophysical Research: Oceans*, 104(C9), pp. 20863-20883. https://doi.org/10.1029/1999JC900139

18. Reynolds, R.W., Smith, T.M., Liu, C., Chelton, D.B., Casey, K.S. and Schlax, M.G., 2007. Daily High-Resolution-Blended Analyses for Sea Surface Temperature. *Journal of Climate*, 20(22), pp. 5473-5496. https://doi.org/10.1175/2007JCLI1824.1

About the authors:

Vladimir A. Pavlushin, research engineer, Marine Hydrophysical Institute of RAS (2 Kapitanskaya Str., Sevastopol, 299011, Russian Federation), **ORCID ID: 0000-0003-0079-7403**, pavlushin.92@mail.ru

Arseny A. Kubryakov, Leading Research Associate, Head of the Laboratory of Innovative Methods and Means of Oceanological Research, Marine Hydrophysical Institute of RAS (2 Kapitanskaya Str., Sevastopol, 299011, Russian Federation), Ph. D. (Phys.-Math.), **ORCID ID: 0000-0003-3561-5913**, arskubr@mhi-ras.ru

Contribution of the co-authors:

Vladimir A. Pavlushin – carrying out the calculations, constructing maps, writing the text of the article

Arseny A. Kubryakov – editing the text of the article, the problem setting

All the authors have read and approved the final manuscript.
The authors declare that they have no conflict of interest.